Published in final edited form as:
Anal Biochem. 2013 November 1; 442(1): . doi:10.1016/j.ab.2013.06.014.

Oxidized Fatty Acid Analysis by Charge Switch Derivatization, Selected Reaction Monitoring and Accurate Mass Quantification

Xinping Liu[1], **Sung Ho Moon**[1], **David J. Mancuso**[1], **Christopher M. Jenkins**[1], **Shaoping Guan**[1], **Harold F. Sims**[1], and **Richard W. Gross**[1,2,3]

[1]Division of Bioorganic Chemistry and Molecular Pharmacology, Department of Medicine, Washington University School of Medicine, St. Louis, MO, USA

[2]Division of Bioorganic Chemistry and Molecular Pharmacology, Department of Developmental Biology, Washington University School of Medicine, St. Louis, MO, USA

[3]Department of Chemistry, Washington University, St. Louis, MO, USA

Abstract

A highly sensitive, specific and robust method for the analysis of oxidized metabolites of linoleic, acid (LA), arachidonic acid (AA) and docosahexaenoic acid (DHA) was developed using charge-switch derivatization, LC-ESI MS/MS with selected reaction monitoring (SRM) and quantitation by high mass accuracy analysis of product ions thereby minimizing interferences from contaminating ions. Charge-switch derivatization of LA, AA and DHA metabolites with N-(4-aminomethylphenyl)-pyridinium resulted in a 10-30 fold increase in ionization efficiency. Improved quantitation was accompanied by decreased false positive interferences through accurate mass measurements of diagnostic product ions during SRM transitions by ratiometric comparisons with stable isotope internal standards. The limits of quantification (LOQ) were between 0.05 to 6.0 pg with a dynamic range of 3-4 orders of magnitude (correlation coefficient $r^2 > 0.99$). This approach was utilized to quantitate the levels of representative fatty acid metabolites from WT and $iPLA_2\gamma^{-/-}$ mouse liver identifying the role of $iPLA_2\gamma$ in hepatic lipid 2nd messenger production. Collectively, these results demonstrate the utility of high mass accuracy product ion analysis in conjunction with charge-switch derivatization for the highly specific quantitation of diminutive amounts of LA, AA and DHA metabolites in biologic systems.

Keywords

Eicosanoids; Docosanoids; Metabolite Determination; LC-MS/MS; Phospholipase; $iPLA_2\gamma$

Introduction

Polyunsaturated fatty acids (PUFAs) such as arachidonic acid (AA, 20:4n-6), docosahexaenoic acid (DHA, 22:6n-3) and linoleic acid (LA, 18:2n-6) are essential components of mammalian membranes that serve multiple roles in cellular function [1-5].

Address correspondence to: Richard W. Gross, M.D., Ph.D., Washington University School of Medicine, Division of Bioorganic Chemistry and Molecular Pharmacology, 660 South Euclid Avenue, Campus Box 8020, St. Louis, Missouri 63110, Tel. 314 362-2690; FAX 314 362-1402; rgross@wustl.edu.

Typically, these polyunsaturated fatty acids are stored in an inactive form esterified to membrane phospholipids and are released during cellular activation by a wide variety of phospholipases to facilitate cellular responses to external perturbations [6-10]. The precise complement of lipid 2nd messengers in each cell type is determined, in large part, by the integrated array of cell type-specific phospholipases and the kinetic flux through specific downstream oxidative pathways tailored to the function of each cell type to generate a highly specific array of polyunsaturated oxidized signaling metabolites. Prominent examples of oxidative enzymes leading to the generation of signaling fatty acids include the cyclooxygenases [11, 12], lipoxygenases [13-15] and P450 monooxygenases [16, 17]. Many hundreds to thousands of oxidized fatty acid metabolites are generated in mammalian cells that coordinate physiologic signaling processes and cellular adaptation in health, but are subject to maladaptive alterations in disease processes promoting disease progression [18-20]. Accordingly, a major goal of lipid 2nd messenger research is the identification of the diversity of oxidized fatty acids in biologic systems, quantitation of alterations in their amounts during physiologic and pathologic perturbations, and mechanistic identification of their roles in disease processes [e.g., 21-29].

Recent approaches for the identification and quantification of the diversity of oxidized fatty acids in biologic systems have largely relied on liquid chromatographic separation followed by electrospray ionization in the negative ion mode and selected reaction monitoring (SRM) [30-38]. However, ionization in the negative ion mode is inefficient in comparison to ionization in the positive ion mode. Although oxidized fatty acids in inflammatory cells, abscesses, exudates or inflammatory fluids can be measured using negative mode ionization [39-51], the much lower abundance of oxidized fatty acid signaling metabolites that regulate cellular function in muscle, liver, brain and other solid organs are typically 20 - 2000 fold lower than that present in inflammatory cells or fluids. Thus, the substantially lower ionization efficiency in the negative ion mode has placed severe limitations on the accurate identification and quantitation of oxidized fatty acids in non-inflammatory cells and tissues.

The inherent limitations in sensitivity in the analysis of oxidized fatty acids in the negative ion mode have previously been appreciated. Accordingly, multiple charge-switch chemical derivatization procedures to improve the ionization efficiency for detection of oxidized fatty acid signaling metabolites have been developed using derivatization and positive ion mode ionization [e.g., 52-59]. Examples of charge switch derivatization of the carboxylic acid group include derivatization with tris(2,4,6-trimethoxyphenyl)phosphonium propylamine (TMPP) bromide [52], cholamine [53], 2-bromo-1-methylpyridinium iodide (BMP) and 3-carbinol-1-methylpyridinium iodide (CMP) [54], p-dimethylaminophenacyl bromide (DmPA-Br) [55], 2-Hydrazinopyridine (HP), 2-picolylamine (PA) and others [56-58]. However, these approaches are suboptimal for analysis of oxidized fatty acid moieties using ESI due to the undesirable fragmentation of the charge switch tag in many cases. This weakness was recognized by Gelb *et al.* who utilized molecular orbital calculations to develop a novel charge-switch reagent, N-(4-aminomethylphenyl)-pyridinium (AMPP) [59], which possessed the desired charge switch mediated increase in S/N and markedly improved the generation of informative fragment ions. Through using high mass accuracy product ion analysis in conjunction with AMPP charge–switch derivatization we demonstrate the sensitivity and specificity of this method for the detection and quantitation of oxidized linoleic, arachidonic, and docosahexaenoic acid metabolites in the high attomole and low fmol range. Furthermore, high mass accuracy analysis of diagnostic product ions collected during SRM dramatically decreases false positive interferences which compromise identification and quantitation of the targeted analytes that would otherwise go undetected or over estimated using traditional isobaric SRM analyses. The utility of this approach in biological tissues was examined in hepatic tissue from wild-type and iPLA$_2\gamma^{-/-}$ mice we previously generated and characterized [60-62]. Collectively, this approach provides a facile

method to dramatically increase the sensitivity and accuracy of analysis of diminutive amounts of oxidized fatty acids in biologic samples while simultaneously decreasing false positive interferences through the use of high mass accuracy product ion analysis during monitored SRM transitions.

Materials and Methods

Materials

The following standards from Cayman Chemical (Ann Arbor, MI) were used: thromboxane B_2 (TXB_2), TXB_2-d_4, 6-keto prostaglandin $F_{1\alpha}$ (6keto-$PGF_{1\alpha}$), prostaglandin $F_{2\alpha}$ ($PGF_{2\alpha}$), prostaglandin $F_{1\alpha}$ ($PGF_{1\alpha}$), prostaglandin E_2 (PGE_2), PGE_2-d_4, prostaglandin E_1 (PGE_1), prostaglandin D_2 (PGD_2), leukotriene B_4 (LTB_4), LTB_4-d_4, 5-hydroxy-6E,8Z,11Z,14Z-eicosatetraenoic acid (5-HETE), 8-hydroxy-5Z,9E,11Z,14Z-eicosatetraenoic acid (8-HETE), 11-hydroxy-5Z,8Z,12E,14Z-eicosatetraenoic acid (11-HETE), 12-hydroxy-5Z,8Z,10E,14Z-eicosatetraenoic acid (12-HETE), 12-HETE-d_8, 15-hydroxy-5Z,8Z,11Z,13E-eicosatetraenoic acid (15-HETE), 20-hydroxy-5Z,8Z,11Z,14Z-eicosatetraenoic acid (20-HETE), 5(6)-epoxy-8Z, 11Z,14Z-eicosatrienoic acid (5,6-EET), 8(9)-epoxy-5Z,11Z,14Z-eicosatrienoic acid (8,9-EET), 11(12)-epoxy-5Z,8Z,14Z-eicosatrienoic acid (11,12-EET), 14(15)-epoxy-5Z,8Z,11Z-eicosatrienoic acid (14,15-EET), arachidonic acid (AA), 9-hydroxy-10E,12Z-octadecadienoic acid (9-HODE), 13-hydroxy-9Z,11E-octadecadienoic acid (13-HODE), 13-HODE-d_4, 9-oxo-10E,12Z-octadecadienoic acid (9-OxoODE), 13-oxo-9Z,11E-octadecadienoic acid (13-OxoODE), 9(10)-dihydroxy-12Z-octadecenoic acid (9,10-DiHOME), 9,10-DiHOME-d_4, 12,13-dihydroxy-9Z-octadecenoic acid (12,13-DiHOME), 12,13-DiHOME-d_4, 9(10)-epoxy-12Z-octadecenoic acid (9(10)-EpOME), 12(13)epoxy-9Z-octadecenoic acid (12(13)-EpOME), linoleic acid (LA), 4-hydroxy-5E,7Z, 10Z,13Z,16Z,19Z-docosahexaenoic acid (4-HDoHE), 7-hydroxy-4Z,8E,10Z,13Z,16Z,19Z-docosahexaenoic acid (7-HDoHE), 8-hydroxy-4Z,6E,10Z, 13Z,16Z,19Z-docosahexaenoic acid (8-HDoHE), 10-hydroxy-4Z,7Z,11E,13Z,16Z,19Z-docosahexaenoic acid (10-HDoHE), 11-hydroxy-4Z,7Z,9E,13Z,16Z,19Z-docosahexaenoic acid (11-HDoHE), 13-hydroxy-4Z, 7Z,10Z,14E,16Z,19Z-docosahexaenoic acid (13-HDoHE), 14-hydroxy-4Z,7Z,10Z,12E,16Z, 19Z-docosahexaenoic acid (14-HDoHE), 16-hydroxy-4Z,7Z,10Z, 13Z,17E,19Z-docosahexaenoic acid (16-HDoHE), 19,20-dihydroxy-4Z,7Z,10Z,13Z,16Z-docosapentaenoic acid (19,20-DiHDPA), 10,17-dihydroxy-4Z,7Z,11E,13Z,15E,19Z-docosahexaenoic acid (10,17-DiHDoHE), 7S,8R,17S-trihydroxy-4Z,9E,11E,13Z,15E,19Z-docosahexaenoic acid (RvD1), 7S,16R,17S-trihydroxy-4Z,8E,10Z,12E,14E,19Z-docosahexaenoic acid (RvD2), and docosahexaenoic acid (DHA). AMPP was obtained from Alchem Laboratories Corporation (Alachua, FL). HPLC-grade acetonitrile, methanol, chloroform, and water were purchased from Burdick & Jackson (Muskegon, MI). Glacial acetic acid and N, N-dimethylformamide were obtained from Sigma-Aldrich (St Louis, MO) while N-hydroxybenzotriazole and 3-(dimethylamino)propyl)-ethyl carbodiimide hydrochloride were purchased from Advanced Chem Tech (Louisville, KY) and TCI America (Portland, OR), respectively. Ascentis Express C18 reverse phase high performance liquid chromatography (HPLC) columns (15cm × 2.1mm) were obtained from Supelco (Bellefonte, PA) while solid phase extraction Strata-X columns were purchased from Phenomenex (Torrance, CA).

Preparation of Standard Solutions and Quantitation

Stock solutions of reference standards were prepared at a concentration of 10-100 pg/μl in ethanol and stored in a brown glass vial under nitrogen at −80°C. The stock solutions were further diluted by ethanol to prepare standard working solutions. Appropriate amounts of internal standards of oxidized fatty acids in ethanol were injected into samples (e.g., biologic tissues and fluids) for quantitative analysis by ratiometric comparisons of the high mass

accuracy diagnostic product ion areas to authentic standards. All samples were flash frozen and stored at −180°C prior to polytron homogenization at 0-4°C.

Hepatic Tissue Samples Preparation

Oxidized fatty acids were analyzed in hepatic tissue obtained from either control C57BL/6 mice or in C57BL/6 mice in which $iPLA_2\gamma$ was globally deleted by removal of the active site in exon 5 by homologous recombination as described previously [60]. All animal breeding, care and sacrifice were carried out by protocols approved by the Animal Studies Committee at Washington University School of Medicine. Following sacrifice, livers were immediately removed, quickly rinsed twice in ice-cold PBS (pH7.4) solution, blotted, snap-frozen in liquid nitrogen and stored at −180°C until homogenization and extraction. Samples were polytron homogenized at 0-4°C prior to extraction using a modified Bligh and Dyer procedure. Briefly, ~20 mg of hepatic tissue was extracted by addition of 2 ml of ice-cold MeOH/$CHCl_3$ (1:1 v/v containing 2% HAc) followed directly by addition of 2 μl of an antioxidant mixture (0.2 mg/ml BHT, 0.2 mg/ml EDTA, 2 mg/ triphenylphosphine, and 2 mg/ml indomethacin in a solution of 2:1:1 methanol/ ethanol/H_2O) and stable isotope internal standards (e.g., TXB_2-d_4, LTB_4-d_4,13-HODE-d_4, 9,10-DiHOME-d_4, 12,13-DiHOME-d_4, PGE_2-d_4, and 12-HETE-d_8). Next, the samples were polytron homogenized (at 0-4°C as described above), 1 ml of ice-cold H_2O was added and the resultant mixture was centrifuged at 15,000g for 15 min to separate the organic and aqueous phases. The $CHCl_3$ layer was transferred to a new tube while the aqueous layer was re-extracted by subsequent addition of 1 ml $CHCl_3$, vortexed and layers were separated by centrifugation at 15,000g for 15 min. The $CHCl_3$ extracts were combined, evaporated under a nitrogen stream and resuspended in 1 ml of 10% methanol/water for solid phase extraction.

Solid Phase Extraction

The sample extracts were immediately applied to a Strata-X solid phase extraction cartridge (30 mg/1ml) that had been previously preconditioned with 1 ml of methanol followed by sequential washing with 1 ml of 10% methanol/90% H_2O and 2×1 ml of 5% methanol/95% H_2O. The oxidized fatty acid metabolites were eluted with 2×0.5 ml washes with methanol containing 1% glacial acetic acid. The combined methanol washes were evaporated to dryness using a SpeedVac concentrator prior to charge-switch derivatization with N-(4-aminomethylphenyl)-pyridinium (AMPP).

Derivatization Reactions

Derivatization with AMPP was performed as previously described in detail by Gelb *et al.* [59]. In brief, 15 μl of ice-cold acetonitrile/N,N-dimethylformamide (4:1, v:v) and 15 μl of ice-cold 640 mM (3-(dimethylamino)propyl)ethyl carbodiimide hydrochloride in HPLC grade water were added to the residue in the sample vial. The vial was briefly vortexed and 30 μl of 5 mM N-hydroxybenzotriazole /15 mM AMPP in acetonitrile were added, vortexed and placed in a 60°C water bath for 30 min. Samples were then cooled down and kept in the autosampler rack at 4 °C while queued for injection.

LC-ESI MS/MS Analysis

LC-ESI MS/MS analysis was performed using an LTQ-Orbitrap mass spectrometer (Thermo Scientific, San Jose, CA) equipped with a Surveyor HPLC system (Thermo Scientific, San Jose, CA). Briefly, the derivatized metabolites were separated on a C18 reversed phase column (Ascentis Express, 2.7 μm particles, 150 × 2.1 mm) at 23°C using a linear gradient of solvent A (0.1% glacial acetic acid in water) and solvent B (0.1% glacial acetic acid in acetonitrile) at a flow rate of 0.2 ml/min. The following solvent gradient program was used: 0.0-5.0 min, 25% B; 5.0-7.0 min, 25-35% B; 7.0-20.0 min, 35-60% B; 20.0-20.1 min,

60-100% B; 20.1-24.0 min, 100% B; 24.0-25.0 min, 100% B to 25% B and 10 min isocratic hold at 25% B. The sample injection volume was 10 μl and the autosampler tray temperature was kept at 4°C throughout the analysis. Diagnostic product ion transitions were determined by full mass scans of targeted metabolites to identify informative transitions to monitor during chromatography. Quantitative analysis of the derivatized fatty acids metabolites was performed using LC-MS/MS by ratiometric comparisons of the high mass accuracy (< 5ppm) diagnostic product ions in samples to that of stable isotope internal standards.

Mass spectrometric analyses were carried out on an LTQ-Orbitrap mass spectrometer (Thermo Scientific, San Jose, CA). The LTQ ion source was operated in positive ion mode at sheath, auxiliary, and sweep gas flows (arbitrary units) of 40, 5, and 1, respectively. The capillary temperature was set to 275°C and the electrospray voltage was 4.0 kV. Capillary voltage and the tube lens voltage were set to 2 and 100 V, respectively. Resolving powers (at *m/z* 400 Th) of 30,000 in full scan mode and 7500 in MS/MS mode were used. The instrument was calibrated externally following the manufacturer's instructions and mass accuracy was within 3 ppm at mass values from *m/z* 130 to 2000. For MS/MS analyses, a normalized collision energy of 30% was applied, the activation time was set at 30 ms with an activation parameter q = 0.25. Collision induced dissociation of derivatized oxidized fatty acid metabolites was initially performed by direct infusion of standards and analysis of full mass scan product ion spectra to identify diagnostic transitions. The identified informative precursor and product ion transitions were monitored by isolating the precursor and product ions within a range of ±1 Th. Product ions were collected in the C trap prior to injection into the Orbitrap for accurate mass analysis and ions within 5ppm of the exact mass of the targeted compound were quantified. AGC target settings for FT full mass scan, FT MS2 scan and ion trap MS2 scan were 5×10^5, 2×10^5 and 1×10^4, respectively. Data acquisition was performed using the Xcalibur operating system, Version 2.1 (Thermo Scientific).

Calibration Standards and Quantification

Data analysis was performed using Xcalibur Version 2.1 software. The linearity of the developed method was determined using calibration curves constructed from each of the authentic standards of the targeted metabolites. Metabolite quantitation was performed from ratiometric comparisons of accurate mass measurements corresponding to the accurate mass peak area of the metabolite to the accurate mass peak areas of stable isotope internal standards. Linear regression analysis determined r^2 values of 0.99 or greater for each metabolite.

Statistical Analysis

Statistical analysis was performed using the two-tailed Student's *t* test. *P* values of less than 0.05 were considered to be statistically significant. All data are reported as the mean ±SEM unless otherwise noted.

Results and Discussion

Development of LC-ESI MS/MS Methods for the Analysis of Oxidized Metabolites of Linoleic Acid, Arachidonic Acid and Docosahexaenoic Acid

First, authentic standards of LA, AA and DHA metabolites were extracted, derivatized with AMPP and prepared for mass spectrometric analysis by solid phase extraction as described in "Materials and Methods." The RPHPLC separation of the AMPP-derivatized metabolites of LA, AA and DHA demonstrated excellent chromatographic characteristics during separation on a C18 reversed phase column at 23°C (Fig. 1). Next, each of the targeted oxidized fatty acid metabolites were analyzed by SRM in the LTQ and product ions resulting from diagnostic transitions were collected in the C trap. Product ions from each

monitored transition were injected into the Orbitrap for accurate mass determination (<5ppm) to minimize false positive interferences. Examination of each of the representative oxidized derivatized fatty acid metabolites demonstrated full mass product ion fragmentation patterns in the LTQ Orbitrap that were similar to those using QqQ instruments [59], but differed substantially in the relative abundance of each of the product ions produced. This result is consistent with the differing modes of fragmentation produced in ion traps which induce bond cleavage by RF excitation *vs*. fragmentation in QqQ instruments which induce fragmentation by collisional activation with inert gases.

The separation of AMPP charge-switch derivatized oxidized fatty acid products was optimized using a customized mobile phase gradient (described in "Materials and Methods") which resulted in baseline resolution of the majority of targeted metabolites (Fig. 1). Diagnostic fragmentation products of the authentic standards of the targeted analytes were first identified using direct infusion and subsequently substantiated by fragmentation of column chromatographic eluents. Each of the oxidized fatty acids examined were either baseline resolved by RPHPLC or analytes that possessed overlapping chromatographic retention times were discriminated based on diagnostic SRM transitions. Ions corresponding to the monitored transitions were collected in the C trap and injected into the Orbitrap for accurate mass determination to minimize false positive interferences that are not related to the analyte of interest.

As previously discussed by Gelb *et al.* [59] the utility of the AMPP derivatization lies not only in its salutary effects of increased ionization efficiency from charge-switch derivatization that result in increased S/N, but moreover facilitates the accrual of multiple informative fragment ions that emanate from dual mechanisms of fragmentation of the AMPP tag. Specifically, the AMPP derivatization tag yielded markers for metabolites of derivatized fatty acids through monitoring the high mass accuracy fragmentation of the diagnostic ions present at *m/z* 183.0917 (benzenemethanimine pyridinium ion) and *m/z* 169.0886 (tolylpyridinium distonic radical ion) that can physically map the elution profile of candidate derivatized fatty acid metabolites as well as other metabolites containing a carboxylic group present during extraction (Scheme 1).

The salutary design of AMPP tag not only delivers markedly enhanced sensitivity but also results in concomitant fragmentations in both the analyte and tag portions as was envisioned using molecular orbital calculations performed by Gelb *et al.* [59]. As anticipated, this strategy works extremely well with multiple other oxidized fatty acid metabolites of great biologic significance. In some cases, chromatographic elution results in the incomplete resolution of metabolites with similar structures. To circumvent this difficulty, we identified diagnostic transitions that can be utilized to discriminate metabolites that are incompletely resolved. For example, 16- and 17-HDoHE as well as 10- and 11-HDoHE possessed overlapping chromatographic elution profiles which were discriminated by high mass accuracy determination of diagnostic product ions. Specifically, the unique transition in 16-HDoHE (*m/z* 511→ *m/z* 401, Fig. 2A) was not present in the coeluting 17-HDoHE (*m/z* 511→ *m/z* 441, Fig. 2B) thus allowing discrimination between each coeluting metabolite. As proposed in Scheme 2, formation of the ion at *m/z* 401.2587 likely results from the loss of 2, 4-heptadienal ($C_7H_{10}O$) from 16-HDoHE-AMPP).

Similarly, the product ion at *m/z* 441.2537 was likely generated from the loss of 2-pentene (C_5H_{10}) from 17-HDoHE-AMPP. The unique transition of *m/z* 511→ *m/z* 321 for 10-HDoHE (Fig.3A) was selected to discriminate the coeluting metabolite 11-HDoHE for which the identified diagnostic transition of *m/z* 511→ *m/z* 361 was employed (Fig. 3B). The proposed fragmentation pathways for formation of the *m/z* 321.1961 and *m/z* 361.1911

ions from 10- and 11-HDoHE AMPP amides, due to loss of $C_{13}H_{18}O$ and $C_{11}H_{18}$, respectively, are shown in Scheme 3.

Accurate mass determination of product ions derived from SRM can substantively reduce false positive identifications. We and others [37] have identified difficulties in metabolite identification and quantitation using precursor and product ions with 1Th selection windows which have the potential to contain multiple different isobaric analytes/interferences in addition to the analyte of interest. In many cases, utilization of SRM results in relatively pure product ions as assessed by accurate mass determination. For example over 99% of murine 12-HETE in serum was authenticated by product ion accurate mass analysis thereby substantiating the integrity of the measured analyte using conventional procedures (Fig. 4A and B). In contrast, when a sample of mouse serum was analyzed for PGE_1 using the identified SRM transition of *m/z* 521 → *m/z* 493 eluting with retention time 9.3 min (Fig. 4C and D), the resulting product ions from SRM demonstrated that although the majority of the product ions at the monitored transition were likely authentic PGE_1 (exact mass=493.3425), two contaminating ions were also present at m/z 492.8650 and 492.5438 (each markedly outside of the 5 ppm accurate mass selection window). Calculations of the combined areas of the two contaminating peaks to that of authentic PGE_1 demonstrated that an error of 27% was introduced by the presence of the contaminating ions. Accurate mass from SRM product ion determination eliminates the interfering ions at *m/z* 492.8650 and 492.5438, thereby providing more accurate quantitative results. Another example of the utility of accurate mass product ion analysis is demonstrated in the false positive identification of LTB4 from mesenteric arteries (Fig. 4E and 4F). Using accurate mass analysis of the product ions generated during the monitored SRM transition (m/z 503→ m/z 391) clearly eliminated the interference of the contaminating ion present at *m/z* 391.3361. This erroneous assignment of this ion contributes 44% of the total peak area that would be obtained using unit mass resolution during conventional isobaric SRM analysis. These results were not due to alterations resulting from the changes in the mode of ionization (negative to positive) or the derivatization reaction since false positive identification of 13,14-dihydro15keto $PGF_{2\alpha}$ were previously documented in underivatized samples using RPHPLC and LC-MS/MS with SRM in the negative ion mode. Specifically, Volmer *et al.* reported that the ion peak at *m/z* 113 which was identified as 13,14-dihydro15keto $PGF_{2\alpha}$ in chronic lymphocytic leukemia cells using SRM (*m/z* 353 → *m/z* 113) with unit mass resolution represented a false positive identification (Fig. 2;[37];)**.** We have observed multiple similar errors in identification and quantitation using conventional SRM analysis with isobaric product ion determination which can be deconvoluted using product ion accurate mass analysis. In many cases this problem is more significant, affecting not only quantitation, but leading to false identification of the observed ion peak. For example (Fig. 5), when a sample of a murine mesenteric artery was analyzed for LTB_4 (*m/z* 503 → *m/z* 391, retention time 10.45min), the results demonstrated abundant product ions resulting from this transition leading to the conclusion that LTB_4 was present in mesenteric arteries. However, the accurate mass of the monitored product ion does not correspond to that of the product ion of LTB_4 standard (i.e. *m/z* 391.2016) while the spiked authentic deuterated internal standard LTB_4 was present in the anticipated amount as assessed by accurate mass (product ion accurate mass 393.2142 resulting from the transition of tetra deuterated LTB_4 *m/z* 507 → *m/z* 393) (spectrum not shown). Thus, high mass accuracy determination eliminates the false positive identification of LTB_4 that cannot be revealed using SRM with isobaric mass resolution. Thus, one approach to minimize false positive interferences is the use of high mass accuracy analysis of product ions collected during the monitored SRM transitions. Product ions which do not match the accurate mass of their isobarically assigned analytes do not represent the moiety of interest and instead may be generated in a variety of ways from different known and unknown metabolites, their fragmentation products or

products from sequential fragmentations to give rise to unanticipated product ions during SRM analysis that do not result from the analyte of interest.

Recovery of Metabolites during Solid Phase Extraction, Linearity of Quantitation and the Limits of Quantitation Using High Mass Accuracy Product Ion Analysis

Recoveries of metabolites from Strata-X cartridges were measured following the extraction of samples of each metabolite by ratiometric comparison to high mass accuracy measurements of stable isotope internal standard. Extraction yields were obtained by comparing the LC-ESI MS/MS peak integrals to those obtained from AMPP derivatized samples that were directly injected onto the LC column. The extraction recoveries for each metabolite were excellent (Table 1). Using the optimized conditions in "Materials and Methods" as described above, the sensitivity, linearity and accuracy of the developed method were examined. Table 1 summarizes the linearity of quantitation, lower limit of quantitation, dynamic range and accuracy of quantitation. The limits of quantitation for LA and AA oxidized metabolites were between 0.05 to 1.0 pg and linear calibration ranges up 300 to 1000 pg were observed. The limits of quantitation for DHA oxidized metabolites were between 0.5 to 6.0 pg with linear calibration ranges up 500 to 1000 pg. Linear regression analysis determined correlation coefficient r^2 values of 0.99 or greater for each analyte. Analytes were quantified using standard curves created through high mass accuracy (<5 ppm) determinations of peak areas of standards by ratiometric comparisons to high mass accuracy product ion determinations of metabolites. The accuracy was calculated as the percentage of measured value to the expected values in quality control samples. Table 1 lists the figures of merit for the developed high mass accuracy charge switch approach for oxidized fatty acid metabolites.

Analysis of the Oxidized Metabolites of LA, AA and DHA in Hepatic Tissues from Wide-Type and iPLA$_2$γ Genetic Knockout Mice

To demonstrate the utility of this approach in biologic samples, oxidized metabolites of LA, AA and DHA in hepatic tissues from wild-type mice and iPLA$_2\gamma^{-/-}$ mice were examined. Using the developed method, we were able to identify and quantitate 37 targeted metabolites derived from LA, AA and DHA in murine liver (Fig. 6). The metabolites from linoleic acid (Fig. 6A) revealed significant decreases for 9(10)- and 12(13)-EpOME as well as their epoxide hydrolase products 9,10-DiHOME and 12,13-DiHOME ($p < 0.05$). In contrast, the hepatic content of 9- and 13-HODE and their allylic hydroxyl oxidization products (9- and 13-oxoODE) were unchanged in WT *vs.* iPLA$_2\gamma^{-/-}$ mice. Analysis DHA metabolites (Fig. 6B) demonstrated specific alterations in hepatic docosanoids after genetic ablation of iPLA$_2\gamma$. These included a 43% decrease of 19,20-DiHDPA which was the major DHA metabolite in liver, a 68% decrease in RvD2 and 17-HDoHE, a 52% decrease in 14-HDoHE, and a 55% decrease in 4-HDoHE. The other measured DHA oxidized molecular species were statistically unchanged in comparisons between iPLA$_2\gamma^{-/-}$ mice and their WT littermates. Additionally, oxidized AA metabolites revealed significant decreases in the content of 5-, 8-, 11-, 12- and 15-HETEs in the iPLA$_2\gamma^{-/-}$ mouse. In contrast, the content of EETs was unchanged in hepatic tissue of the iPLA$_2\gamma^{-/-}$ mouse (Fig. 6C). Significant changes were also found in prostaglandins PGD_2, TXB_2, $PGF_2\alpha$, and 6keto-$PGF_1\alpha$. We also measured the content of non-esterified AA, LA and DHA in WT murine liver (AA, 14.1 ± 2.5 ng/mg; LA, 21.7 ± 4.2 ng/mg; and DHA, 34.8 ± 2.1 ng/mg) as well as liver from iPLA$_2\gamma^{-/-}$ mice (AA, 10.9 ± 1.3 ng/mg; LA, 12.9 ± 1.1 ng/mg; and DHA, 24.8 ± 1.8 ng/mg). The results demonstrated the decreased polyunsaturated fatty acids in iPLA$_2\gamma^{-/-}$ liver and indicate the important role of iPLA$_2\gamma$ in murine liver lipid signaling and metabolism.

Conclusions

The identification and quantitation of diminutive amounts of oxidized fatty acid signaling metabolites in biologic tissues is essential to understanding the roles of lipid 2nd messengers in biologic systems. However, the identification and quantitation of the diminutive amounts of oxidized non-esterified fatty acids in non-inflammatory cells or exudates is challenging task. In this study, we have utilized a high mass accuracy charge-switch approach to gain deep penetrance into the extremely low abundance regime of oxidized fatty acids that enables their identification, improves quantitation and can be effectively multiplexed as the acquisition rate of tandem mass spectra in next generation instrumentation increases. Through the exquisite sensitivity of charge-switch derivatization in conjunction with the judicious use of informative transitions whose integrity is substantiated by high mass accuracy product ions analyses, new insights into the roles of oxidized fatty acids in cellular biology can be accrued.

Acknowledgments

This work was supported, in whole or in part, by National Institutes of Health Grants RO1HL41250 and RO1HL118639. R. W. G. has financial relationships with LipoSpectrum and Platomics.

References

[1]. Benatti P, Peluso G, Nicolai R, Calvani M. Polyunsaturated Fatty Acids: Biochemical, Nutritional and Epigenetic Properties. J. Am. Coll. Nutr. 2004; 23:281–302. [PubMed: 15310732]

[2]. Gillies PJ, Harris WS, Kris-Etherton PM. Omega-3 fatty acids in food and pharma: the enabling role of biotechnology. Curr. Atheroscler. Rep. 2011; 13:467–473. [PubMed: 21892757]

[3]. Jenkins CM, Cedars A, Gross RW. Eicosanoid signaling pathways in the heart. Cardiovasc. Res. 2009; 82:240–249. [PubMed: 19074824]

[4]. Sears B, Ricordi C. Role of fatty acids and polyphenols in inflammatory gene transcription and their impact on obesity, metabolic syndrome and diabetes. Eur. Rev. Med. Pharmacol. Sci. 2012; 16:1137–54. [PubMed: 23047497]

[5]. Zechner R, Zimmermann R, Eichmann TO, Kohlwein SD, Haemmerle G, Lass A, Madeo F. FAT SIGNALS - Lipases and Lipolysis in Lipid Metabolism and Signaling. Cell Metabolism. 2012; 15:279–291. [PubMed: 22405066]

[6]. Gross RW. High plasmalogen and arachidonic acid content of canine myocardial sarcolemma: a fast atom bombardment mass spectroscopic and gas chromatography-mass spectroscopic characterization. Biochemistry. 1984; 23:158–165. [PubMed: 6419772]

[7]. Hazen SL, Ford DA, Gross RW. Activation of a membrane-associated phospholipase A_2 during rabbit myocardial ischemia which is highly selective for plasmalogen substrate. J. Biol. Chem. 1991; 266:629–5633.

[8]. Ford DA, Hazen SL, Saffitz JE, Gross RW. The rapid and reversible activation of a calcium-independent plasmalogen-selective phospholipase A_2 during myocardial ischemia. J. Clin. Invest. 1991; 88:331–335. [PubMed: 2056126]

[9]. Gross RW, Han X. Lipidomics at the Interface of Structure and Function in Systems Biology. Chem. Biol. 2011; 18:284–291. [PubMed: 21439472]

[10]. Ziboh VA, Miller CC, Cho Y. Metabolism of polyunsaturated fatty acids by skin epidermal enzymes: generation of antiinflammatory and antiproliferative metabolites. Am. J. Clin. Nutr. 2000; 71:S361S–366.

[11]. Rouzer CA, Marnett LJ. Cyclooxygenases: structural and functional insights. J. Lipid Res. 2009; 50:S29–34. [PubMed: 18952571]

[12]. Smith WL, DeWitt DL, Garavito RM. Cyclooxygenases: structural, cellular, and molecular biology. Annu. Rev. Biochem. 2000; 69:145–182. [PubMed: 10966456]

[13]. Fürstenberger G, Krieg P, Müller-Decker K, Habenicht AJ. What are cyclooxygenases and lipoxygenases doing in the driver's seat of carcinogenesis? Int. J. Cancer. 2006; 119:2247–2254. [PubMed: 16921484]

[14]. Radmark O, Samuelsson B. 5-Lipoxygenase: mechanisms of regulation. J. Lipid Res. 2009; 50:S40–45. [PubMed: 18987389]

[15]. Pidgeon GP, Lysaght J, Krishnamoorthy S, Reynolds JV, O'Byrne K, Nie D, Honn KV. Lipoxygenase metabolism: roles in tumor progression and survival. Cancer Metastasis Rev. 2007; 26:503–524. [PubMed: 17943411]

[16]. Roman RJ. P-450 metabolites of arachidonic acid in the control of cardiovascular function. Physiol. Rev. 2002; 82:131–185. [PubMed: 11773611]

[17]. Sarkis A, Roman RJ. Role of cytochrome P450 metabolites of arachidonic acid in hypertension. Curr. Drug Metab. 2004; 5:245–256. [PubMed: 15180494]

[18]. Moon SH, Jenkins CM, Liu X, Guan S, Mancuso DJ, Gross RW. Activation of mitochondrial calcium-independent phospholipase A2γ (iPLA2γ) by divalent cations mediating arachidonate release and production of downstream eicosanoids. J. Biol. Chem. 2012; 287:14880–14895. [PubMed: 22389508]

[19]. Greene ER, Huang S, Serhan CN, Penigrahy D. Regulation of inflammation in cancer by eicosanoids. Prostaglandins and Other Lipid Mediators. 2011; 96:27–36. [PubMed: 21864702]

[20]. Funk CD. Prostaglandins and leukotrienes: advances in eicosanoid biology. Science. 2001; 294:1871–1875. [PubMed: 11729303]

[21]. Patwardhan AM, Scotland PE, Akopian AN, Hargreaves KM. Activation of TRPV1 in the spinal cord by oxidized linoleic acid metabolites contributes to inflammatory hyperalgesia. Proc. Natl. Acad. Sci. USA. 2009; 44:18820–18824. [PubMed: 19843694]

[22]. Patwardhan AM, Akopian AN, Ruparel NB, Diogenes A, Weintraub ST, Uhlson C, Murphy RC, Hargreaves KM. Heat generates oxidized linoleic acid metabolites that activate TRPV1 and produce pain in rodents. J. Clin. Invest. 2010; 120:1617–26. [PubMed: 20424317]

[23]. Moghaddam MF, Grant DF, Cheek JM, Greene JF, Williamson KC, Hammock BD. Bioactivation of leukotoxins to their toxic diols by epoxide hydrolase. Nat. Med. 1997; 3:562–566. [PubMed: 9142128]

[24]. Hong S, Gronert K, Devchand PR, Moussignac RL, Serhan CN. Novel docosatrienes and 17S-resolvins generated from docosahexaenoic acid in murine brain, human blood, and glial cells autacoids in anti-inflammation. J. Biol. Chem. 2003; 278:14677–14687. [PubMed: 12590139]

[25]. Bailes JE, Mills JD. Docosahexaenoic acid reduces traumatic axonal injury in a rodent head Injury model. J. Neurotrauma. 2010; 27:1617–1624. [PubMed: 20597639]

[26]. Ariel A, Serhan CN. Resolvins and protectins in the termination program of acute inflammation. Trends Immunol. 2007; 28:176–183. [PubMed: 17337246]

[27]. Spite M, Norling LV, Summers L, Yang R, Cooper D, Petasis NA, Flower RJ, Perretti M, Serhan CN. Resolvin D2 is a potent regulator of leukocytes and controls microbial sepsis. Nature. 2009; 461:1287–1291. [PubMed: 19865173]

[28]. Kasuga K, Yang R, Porter TF, Agrawal N, Petasis NA, Irimia D, Toner M, Serhan CN. Rapid appearance of resolvin precursors in inflammatory exudates: novel mechanisms in resolution. J. Immunol. 2008; 181:8677–8687. [PubMed: 19050288]

[29]. Xu ZZ, Zhang L, Liu T, Park JY, Berta T, Yang R, Serhan CN, Ji RR. Resolvins RvE1 and RvD1 attenuate inflammatory pain via central and peripheral actions. Nat. Med. 2010; 16:592–597. [PubMed: 20383154]

[30]. Takabatake M, Hishinuma T, Suzuki N, Chiba S, Tsukamoto H, Nakamura H, Saga T, Tomioka Y, Kurose A, Sawai T, Mizugaki M. Simultaneous quantification of prostaglandins in human synovial cell-cultured medium using liquid chromatography/tandem mass spectrometry. Prostaglandins Leukot. Essent. Fatty Acids. 2002; 67:51–56. [PubMed: 12213436]

[31]. Deems RA, Buczynski MW, Bowers-Gentry RC, Harkewicz R, Dennis EA. Detection and quantitation of eicosanoids via high performance liquid chromatography/electrospray ionization mass spectrometry. Meth. Enzymol. 2007; 432:59–82. [PubMed: 17954213]

[32]. Harkewicz R, Dennis EA. Applications of mass spectrometry to lipids and membranes. Annu. Rev. Biochem. 2011; 80:301–325. [PubMed: 21469951]

[33]. Buczynski MW, Stephens DL, Bowers-Gentry RC, Grkovich A, Deems RA, Dennis EA. TLR-4 and sustained calcium agonists synergistically produce eicosanoids independent of protein synthesis in RAW264.7 cells. J. Biol. Chem. 2007; 282:22834–22847. [PubMed: 17535806]

[34]. Dickinson JS, Murphy RC. Mass spectrometric analysis of leukotriene A4 and other chemically reactive metabolites of arachidonic acid. J. Am. Soc. Mass Spectrom. 2002; 13:1227–1234. [PubMed: 12387329]

[35]. Zhang J, Pearson T, Matharoo-Ball B, Ortori CA, Warren AY, Khan R, Barrett DA. Quantitative profiling of epoxyeicosatrienoic, hydroxyeicosatetraenoic, and dihydroxyeicosatetraenoic acids in human intrauterine tissues using liquid chromatography/electrospray ionization tandem mass spectrometry. Anal. Biochem. 2007; 365:40–51. [PubMed: 17418798]

[36]. Yang J, Schmelzer K, Georgi K, Hammock BD. Quantitative profiling method for oxylipin metabolome by liquid chromatography electrospray ionization tandem mass Spectrometry. Anal. Chem. 2009; 81:8085–8093. [PubMed: 19715299]

[37]. Masoodi M, Eiden M, Koulman A, Spaner D, Volmer DA. Comprehensive lipidomics analysis of bioactive lipids in complex regulatory networks. Anal. Chem. 2010; 82:8176–8185. [PubMed: 20828216]

[38]. Kita Y, Takahashi T, Uozumi N, Nallan L, Gelb MH, Shimizu T. Pathway-oriented profiling of lipid mediators in macrophages. Biochem. Biophys. Res. Commun. 2005; 330:898–906. [PubMed: 15809081]

[39]. Gregus AM, Doolen S, Dumlao DS, Buczynski MW, Takasusuki T, Fitzsimmons BL, Hua XY, Taylor BK, Dennis EA, Yaksh TL. Spinal 12-lipoxygenase-derived hepoxilin A3 contributes to inflammatory hyperalgesia via activation of TRPV1 and TRPA1 receptors. Proc. Natl. Acad. Sci. U.S.A. 2012; 109:6721–6726. [PubMed: 22493235]

[40]. Patwardhan AM, Scotland PE, Akopian AN, Hargreaves KM. Activation of TRPV1 in the spinal cord by oxidized linoleic acid metabolites contributes to inflammatory hyperalgesia. Proc. Natl. Acad. Sci. U.S.A. 2009; 106:18820–18824. [PubMed: 19843694]

[41]. Gregus AM, Dumlao DS, Wei SC, Norris PC, Catella LC, Meyerstein FG, Buczynski MW, Steinauer JJ, Fitzsimmons BL, Yaksh TL, Dennis EA. Systematic analysis of rat 12/15-lipoxygenase enzymes reveals critical role for spinal eLOX3 hepoxilin synthase activity in inflammatory hyperalgesia. The FASEB J. 2013; 27:1939–1949.

[42]. von Moltke J, Trinidad NJ, Moayeri M, Kintzer AF, Wang SB, van Rooijen N, Brown CR, Krantz BA, Leppla SH, Gronert K, Vance RE. Rapid induction of inflammatory lipid mediators by the inflammasome in vivo. Nature. 2012; 490:107–111. [PubMed: 22902502]

[43]. Dolęgowska B, Blogowski W, Stępniewska J, Safranow K, Jakubowska K, Olszewska M. Presence of glucose in dialyzing fluid and synthesis of selected lipoxygenase-derived eicosanoids during hemodialysis. Int. Urol. Nephrol. 2012; 44:1799–1804. [PubMed: 22127406]

[44]. Thomas CP, Morgan LT, Maskrey BH, Murphy RC, Kühn H, Hazen SL, Goodall AH, Hamali HA, Collins PW, O'Donnell VB. Phospholipid-esterified Eicosanoids Are Generated in Agonist-activated Human Platelets and Enhance Tissue Factor-dependent Thrombin Generation. J. Biol. Chem. 2010; 285:6891–6903. [PubMed: 20061396]

[45]. Schuck RN, Theken KN, Edin ML, Caughey M, Bass A, Ellis K, Tran B, Steele S, Simmons BP, Lih FB, Tomer KB, Wu MC, Hinderliter AL, Stouffer GA, Zeldin DC, Lee CR. Cytochrome P450-derived eicosanoids and vascular dysfunction in coronary artery disease patients. Atherosclerosis. 2013; 227:442–448. [PubMed: 23466098]

[46]. Theken KN, Deng Y, Kannon MA, Miller TM, Poloyac SM, Lee CR. Activation of the acute inflammatory response alters cytochrome P450 expression and eicosanoid metabolism. Drug Metab. Dispos. 2011; 39:22–29. [PubMed: 20947618]

[47]. Gauthier KM, Goldman DH, Aggarwal NT, Chawengsub Y, Falck JR, Campbell WB. Role of arachidonic acid lipoxygenase metabolites in acetylcholine-induced relaxations of mouse arteries. Am. J. Physiol. Heart Circ. Physiol. 2011; 300:H725–H735. [PubMed: 21193584]

[48]. Bukhari IA, Shah AJ, Gauthier KM, Walsh KA, Koduru SR, Imig JD, Falck JR, Campbell WB. 11,12,20-Trihydroxy-eicosa-8(Z)-enoic acid: a selective inhibitor of 11,12-EET-induced relaxations of bovine coronary and rat mesenteric arteries. Am. J. Physiol. Heart Circ. Physiol. 2012; 302:H1574–583. [PubMed: 22307677]

[49]. Zarini S, Murphy RC. Biosynthesis of 5-oxo-6,8,11,14-eicosatetraenoic acid from 5-hydroperoxyeicosatetraenoic acid in the murine macrophage. J. Biol. Chem. 2003; 278:11190–11196. [PubMed: 12547823]

[50]. Maekawa K, Hirayama A, Iwata Y, Tajima Y, Nishimaki-Mogami T, Sugawara S, Ueno N, Abe H, Ishikawa M, Murayama M, Matsuzawa Y, Nakanishi H, Ikeda K, Arita M, Taguchi R, Minamino N, Wakabayashi S, Soga T, Saito Y. Global metabolomic analysis of heart tissue in a hamster model for dilated cardiomyopathy. J. Mol. Cell Cardiol. 2013; 59:76–85. [PubMed: 23454301]

[51]. Moita E, Gil-Izquierdo A, Sousa C, Ferreres F, Silva LR, Valentao P, Dominguez-Perles R, Baenas N, Andrade PB. Integrated Analysis of COX-2 and iNOS Derived Inflammatory Mediators in LPS-Stimulated RAW Macrophages Pre-Exposed to Echium plantagineum L. Bee Pollen Extract. PLoS ONE. 2013; 8:e59131. [PubMed: 23520554]

[52]. Cartwright AJ, Jones P, Wolff JC, Evans EH. Derivatization of carboxylic acid groups in pharmaceuticals for enhanced detection using liquid chromatography with electrospray ionisation tandem mass spectrometry. Rapid Commun. Mass Spectrom. 2005; 19:1058–1062. [PubMed: 15776497]

[53]. Lamos SM, Shortreed MR, Frey BL, Belshaw PJ, Smith LM. Relative quantification of carboxylic acid metabolites by liquid chromatography-mass spectrometry using isotopic variants of cholamine. Anal. Chem. 2007; 79:5143–5149. [PubMed: 17563114]

[54]. Yang WC, Adamec J, Regnier FE. Enhancement of the LC/MS analysis of fatty acids through derivatization and stable isotope coding. Anal. Chem. 2007; 79:5150–5157. [PubMed: 17492837]

[55]. Guo K, Li L. High-performance isotope labeling for profiling carboxylic acid containing metabolites in biofluids by mass spectrometry. Anal. Chem. 2010; 82:8789–8793. [PubMed: 20945833]

[56]. Higashi T, Ichikawa T, Inagaki S, Min JZ, Fukushima T, Toyo'oka T. Simple and practical derivatization procedure for enhanced detection of carboxylic acids in liquid chromatography-electrospray ionization-tandem mass spectrometry. J. Pharm. Biomed. Anal. 2010; 52:809–818. [PubMed: 20376914]

[57]. Pettinella C, Lee SH, Cipollone F, Blair IA. Targeted quantitative analysis of fatty acids in atherosclerotic plaques by high sensitivity liquid chromatography/tandem mass spectrometry. J. Chromatogr. B. 2007; 850:168–176.

[58]. Johnson DW. Alkyldimethylaminoethyl ester iodides for improved analysis of fatty acids by electrospray ionization tandem mass spectrometry. Rapid Commun. Mass Spectrom. 2000; 14:2019–2024. [PubMed: 11085412]

[59]. Bollinger JG, Thompson W, Lai Y, Oslund RC, Hallstrand TS, Sadilek M, Turecek F, Gelb MH. Improved sensitivity mass spectrometric detection of eicosanoids by charge reversal derivatization. Anal. Chem. 2010; 82:6790–6796. [PubMed: 20704368]

[60]. Mancuso DJ, Sims HF, Han X, Jenkins CM, Guan SP, Yang K, Moon SH, Pietka T, Abumrad NA, Schlesinger PH, Gross RW. Genetic ablation of calcium-independent phospholipase $A_2\gamma$ leads to alterations in mitochondrial lipid metabolism and function resulting in a deficient mitochondrial bioenergetic phenotype. J. Biol. Chem. 2007; 282:34611–34622. [PubMed: 17923475]

[61]. Mancuso DJ, Kotzbauer P, Wozniak DF, Sims HF, Jenkins CM, Guan S, Han X, Yang K, Sun G, Malik I, Conyers S, Green KG, Schmidt RE, Gross RW. Genetic Ablation of Calcium-independent Phospholipase $A_2\gamma$ Leads to Alterations in Hippocampal Cardiolipin Content and Molecular Species Distribution, Mitochondrial Degeneration, Autophagy, and Cognitive Dysfunction. J. Biol. Chem. 2009; 284:35632–35644. [PubMed: 19840936]

[62]. Mancuso DJ, Sims HF, Yang K, Kiebish MA, Su X, Jenkins CM, Guan S, Moon SH, Pietka T, Nassir F, Schappe T, Moore K, Han X, Abumrad NA, Gross RW. Genetic Ablation of Calcium-independent Phospholipase $A_2\gamma$ Prevents Obesity and Insulin Resistance during High Fat Feeding by Mitochondrial Uncoupling and Increased Adipocyte Fatty Acid Oxidation. J. Biol. Chem. 2010; 285:36495–36510. [PubMed: 20817734]

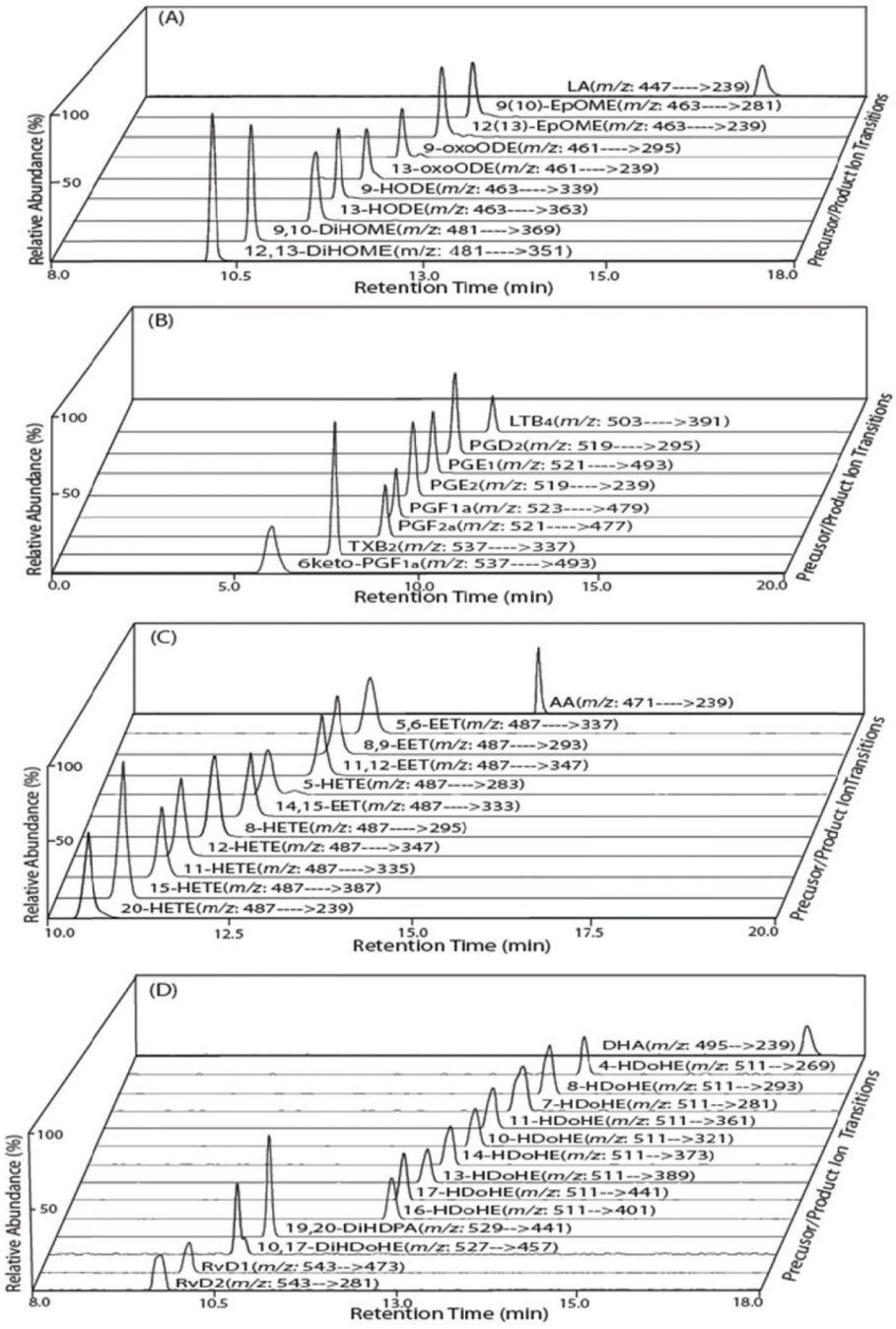

Figure 1. Selected reaction monitoring (SRM) total ion current chromatograms of the targeted oxidized metabolites of linoleic, arachidonic and docosahexaenoic acids

The indicated fatty acid metabolite standards were derivatized with N-(4-aminomethylphenyl)-pyridinium (AMPP) and measured by LC/MS/MS via SRM in the positive ion mode following chromatographic separation using a C18 reverse phase HPLC column as described in “Materials and Methods”. Representative SRM chromatograms for linoleic acid (LA) and the indicated oxidized LA metabolites (A); arachidonic acid (AA) and the indicated oxidized AA metabolites (B and C); and docosahexaenoic acid (DHA) and the indicated oxidized DHA metabolites (D) are shown with their retention times and the informative SRM transitions.

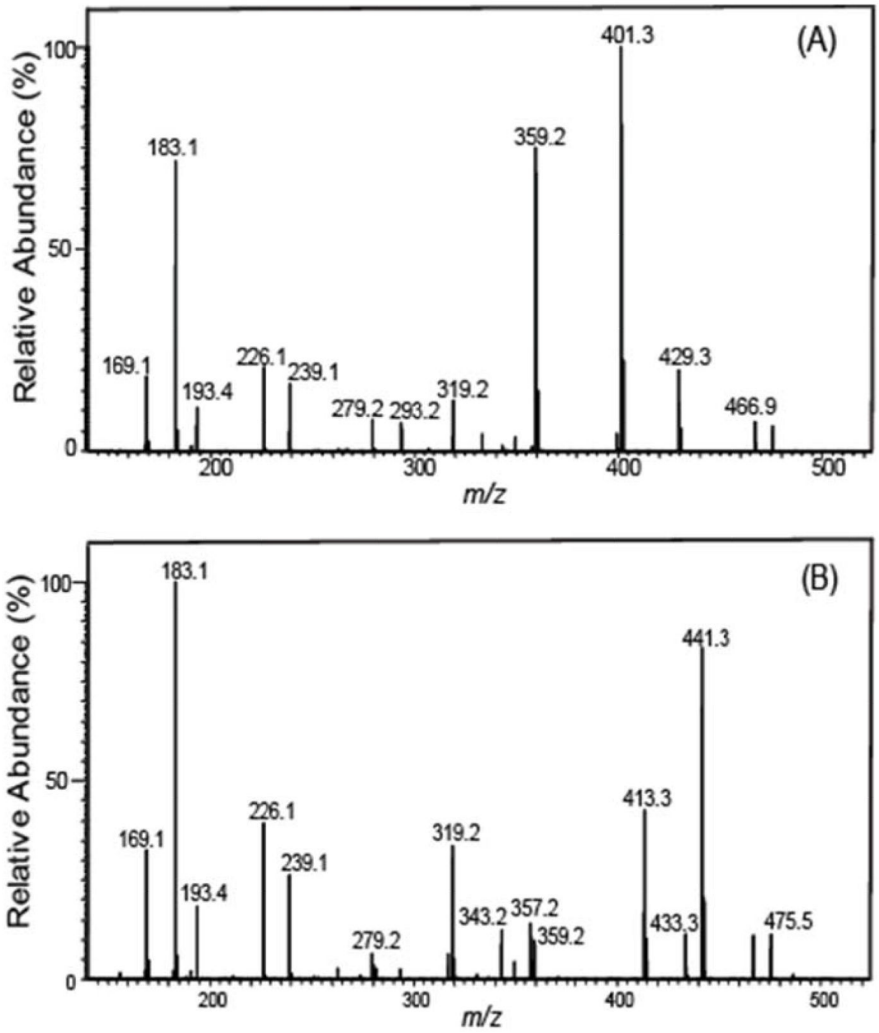

Figure 2. Full mass product ion scans used to discriminate 16- and 17-HDoHE derivatized with N-(4-aminomethylphenyl)-pyridinium (AMPP)

(A) Mass spectrum of the CID of 16-DHoHE-AMPP exhibiting a prominent diagnostic fragment ion at *m/z* 401 which was utilized for the SRM transition based identification and quantitation of 16-DHoHE. (B) Mass spectrum of the CID of 17-DHoHE-AMPP displaying an informative fragment ion at *m/z* 441 which was utilized for the SRM transition based identification and quantitation of 17-DHoHE.

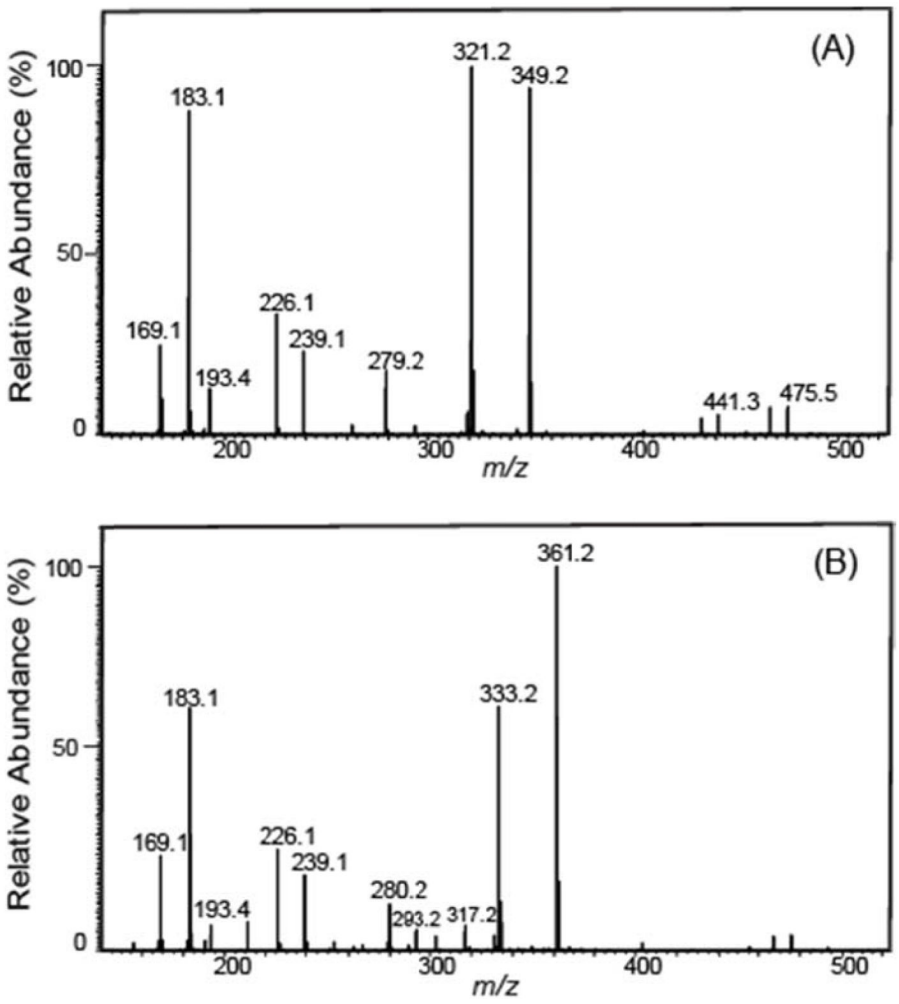

Figure 3. Full mass product ion scans used to discriminate 10- and 11-HDoHE derivatized with N-(4-aminomethylphenyl)-pyridinium (AMPP)

(A) Mass spectrum of the CID of 10-HDoHE-AMPP exhibiting a diagnostic fragment ion at *m/z* 349 which was selected for the SRM transition based identification and quantitation of 10-HDoHE. (B) Mass spectrum of the CID of 11-HDoHE-AMPP displaying an informative fragment ion at *m/z* 361 which was selected for SRM transition based identification and quantitation of 11-HDoHE.

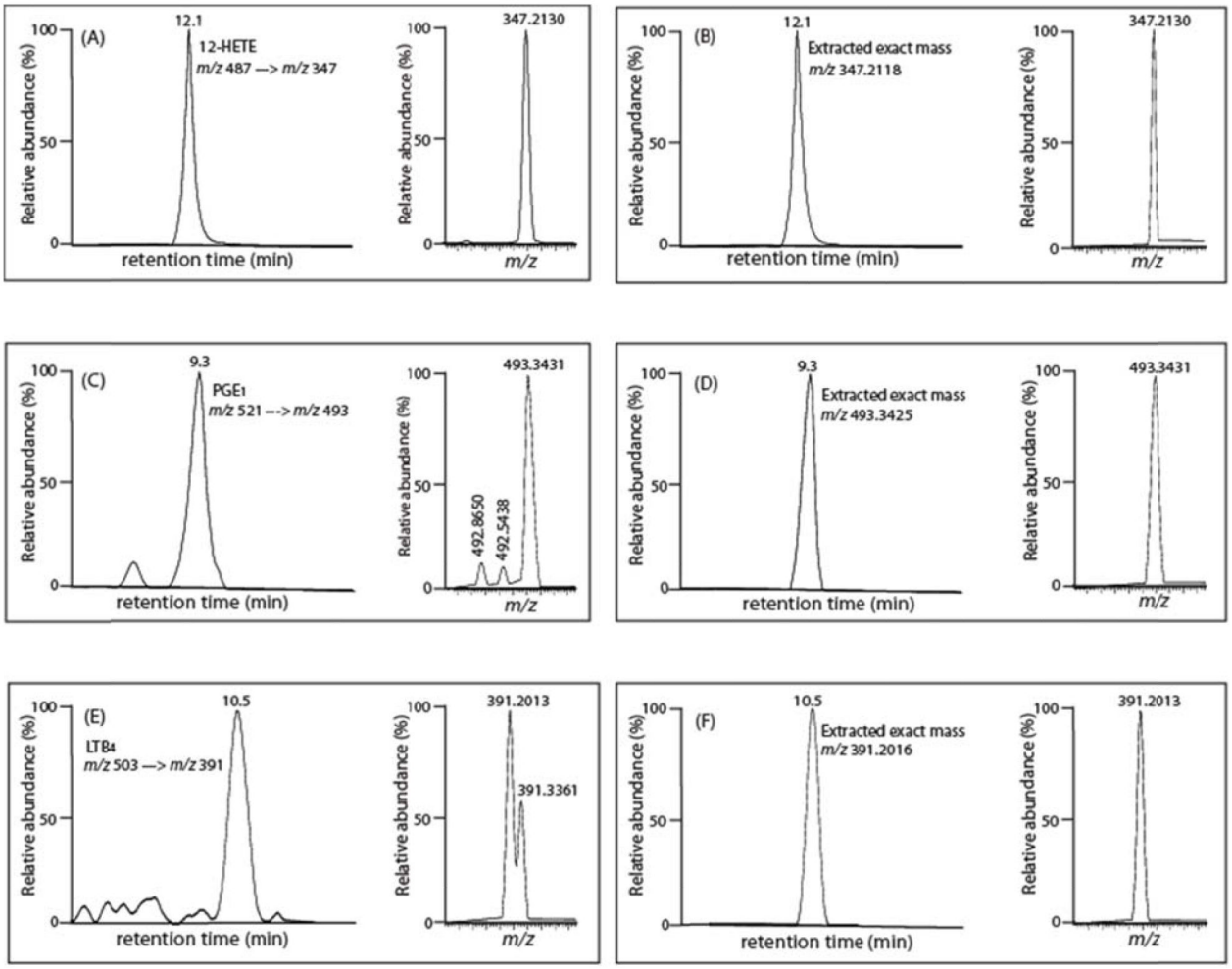

Figure 4. Comparison of quantitative methods for measuring selected eicosanoids in mouse serum using mass unit resolution of product ion SRM and accurate mass product ion SRM

(A) Peak retention time profile and SRM transition (*m*/*z* 487 → *m*/*z* 347) of 12-HETE-AMPP with mass unit resolution; (B) Peak retention time profile and high mass accuracy extracted ion chromatogram of the product ion at *m*/*z* 347.2188 (within 5 ppm); (C): Peak retention time profile and SRM transition (*m*/*z* 521 → *m*/*z* 493) of PGE_1-AMPP with mass unit resolution; (D) Peak retention time profile and high mass accuracy extracted ion chromatogram of the product ion at *m*/*z* 493.3425 (within 5 ppm); (E) Peak retention time profile and SRM transition (*m*/*z* 503 → *m*/*z* 391) of LTB_4-AMPP with mass unit resolution; (F) Peak retention time profile and high mass accuracy extracted ion chromatogram of the product ion at *m*/*z* 391.2016 (within 5 ppm).

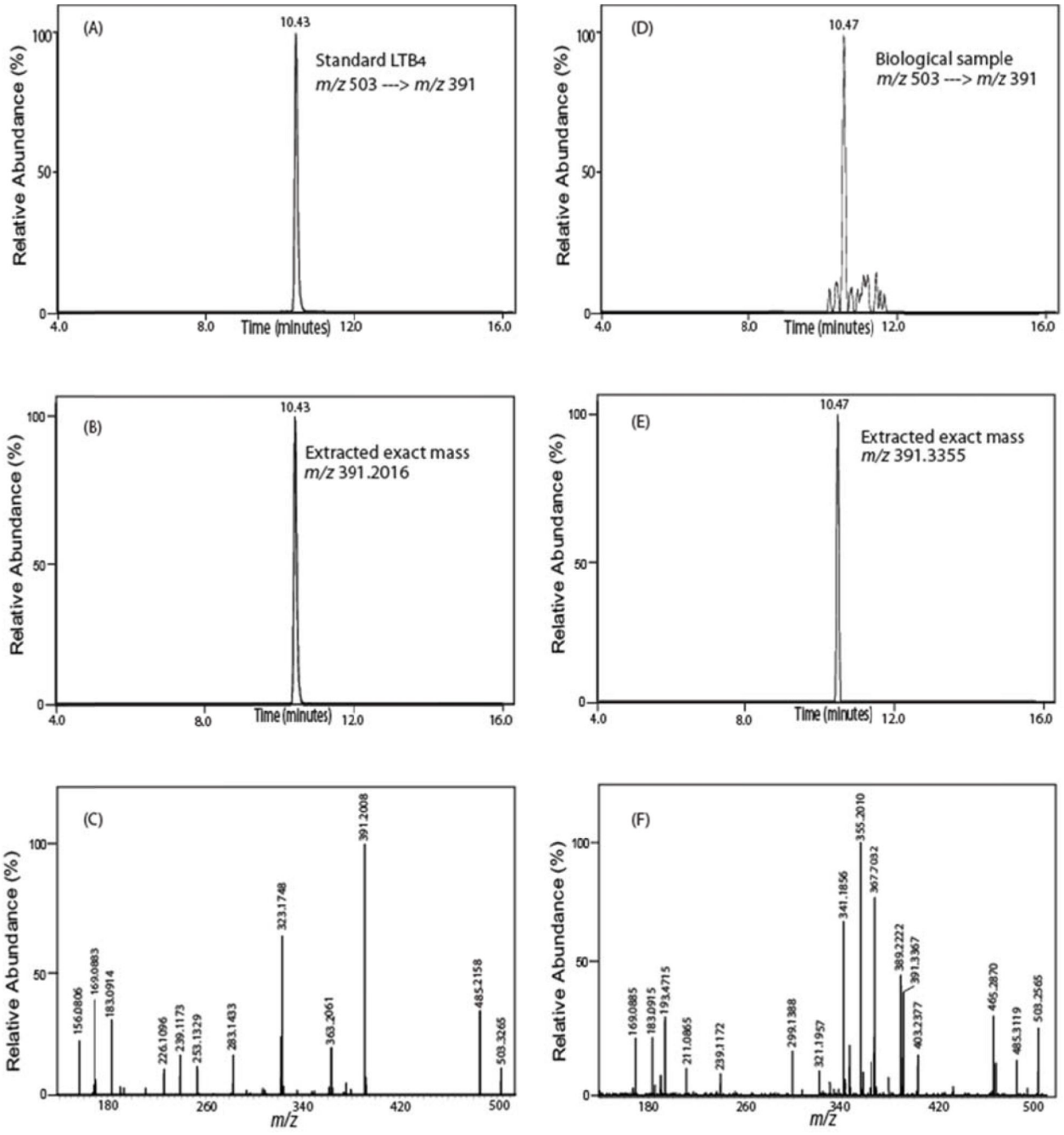

Figure 5. Determination of the false positive identification of LTB_4 in a biologic sample utilizing SRM with accurate product ion mass analyses

(A) Peak retention time profile of LTB_4-AMPP standard utilizing SRM (*m*/*z* 503 → *m*/*z* 391); (B) high mass accuracy extracted ion chromatogram of the product ion, *m*/*z* 391.2016 (within an error of 2 ppm) of the standard LTB_4-AMPP; (C) corresponding full MS/MS spectrum of the LTB_4-AMPP standard; (D) Peak retention time profile indicative of LTB_4-AMPP obtained from murine mesenteric arterial tissue utilizing the SRM transition (*m*/*z* 503 → *m*/*z* 391); (E) high mass accuracy extracted ion chromatogram of the product ion, *m*/*z* 391.3355, present in the biologic sample which does not correspond to the accurate mass of the product ion of LTB_4-AMPP thereby revealing a false positive identification if only mass

unit resolution is utilized (F). The MS/MS spectra of D and E confirm substantial differences between the LTB_4 standard and compounds in the biological sample.

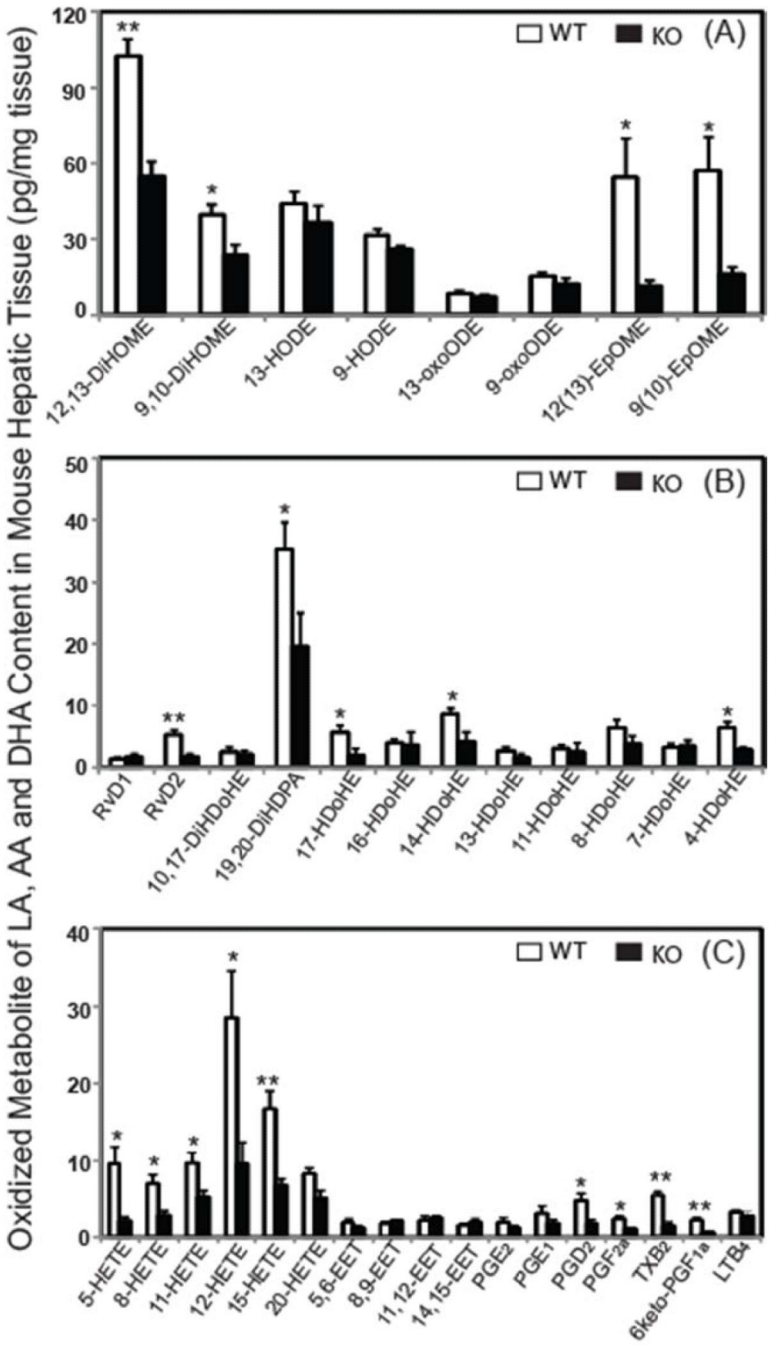

Figure 6. Oxidized metabolites of linoleic acid, arachidonic acid and docosahexaenoic acid in hepatic tissues from wild-type (WT) and iPLA$_2$γ Knockout (KO) mice

Oxidized fatty acid metabolites from murine hepatic tissue were extracted into solvent, isolated by solid phase extraction, derivatized with AMPP and quantitated by LC/MS/MS via selected reaction monitoring (SRM) in the positive ion mode following separation of molecular species using a reverse phase column as described in “Materials and Methods”. Significant decreases in the production of multiple identified oxidized metabolites of LA, DHA and AA as a result of genetic ablation of iPLA$_2$γ are displayed in panels A, B and C, respectively. Values presented are the mean ±S.E. and comparisons were made using Student’s *t*-test (n=4). *: P< 0.05 level, **: P< 0.01 level.

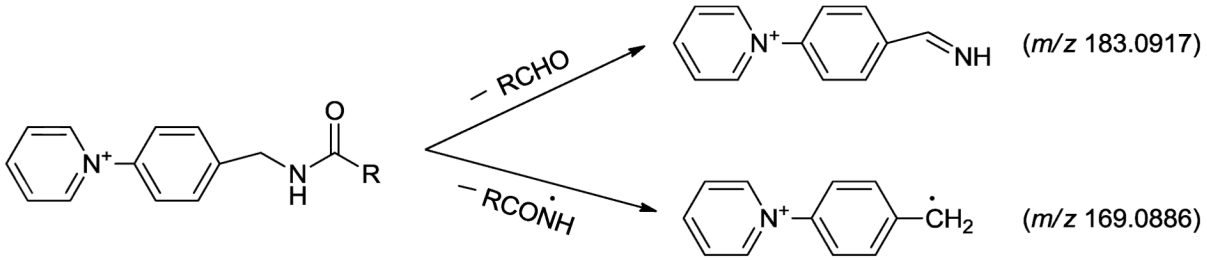

Scheme 1.

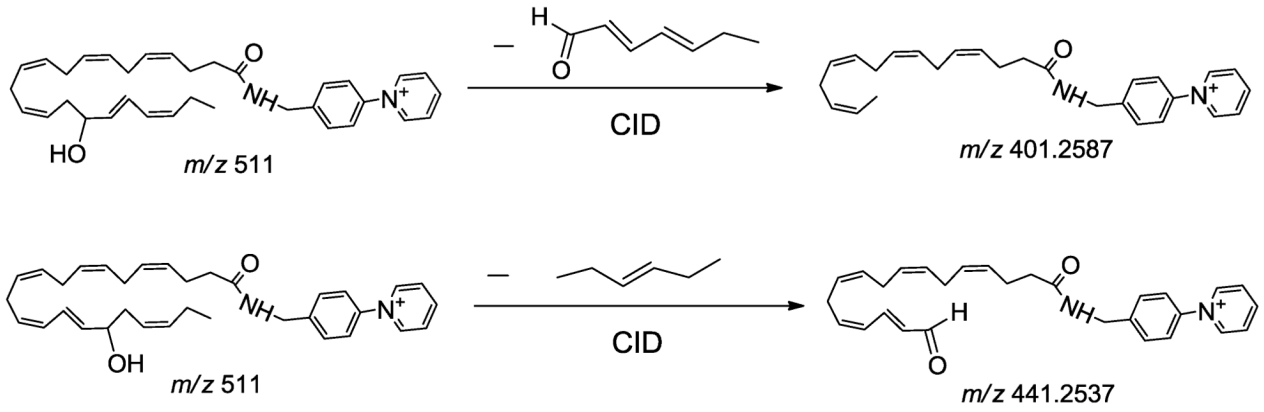

Scheme 2.

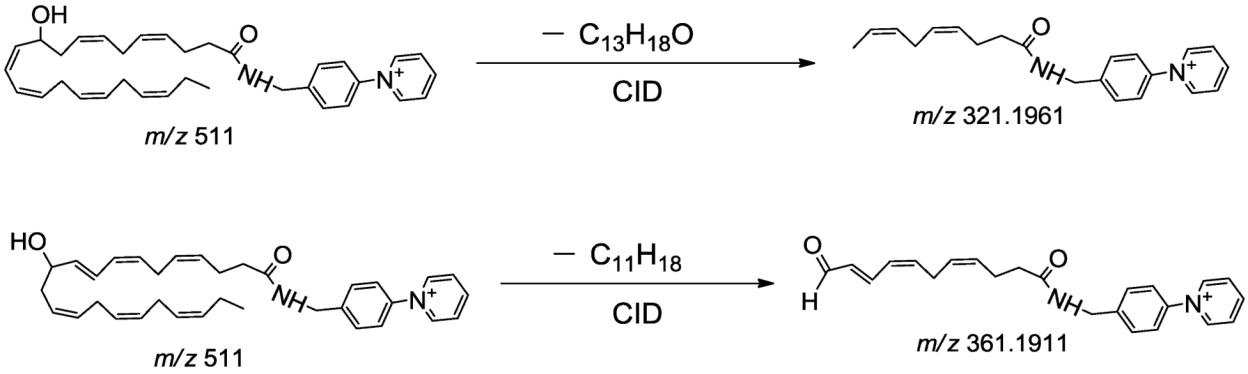

Scheme 3.

Table 1

Relative response factor (R/R_0)[a], linearity of measurement, correlation coefficient (r^2), limits of quantitation (LOQs)[b], extraction yield, and method accuracy[c] analyses

Analytes	Extraction Yield (%)	Accuracy (% ± SD)	R/R_0	LoQ (pg)	Calibrated range (pg)	Correlation coefficient (r^2)	Internal standard
9-HODE	98	95.0 ± 8.5	1.10 ± 0.11	0.05	0.05–300	0.9977	13-HODE-d_4
13-HODE	90	105.0 ± 12.5	1.08 ± 0.08	0.07	0.07–300	0.9956	13-HODE-d_4
9-OxoODE	84	86.2 ± 5.0	0.72 ± 0.05	0.5	0.5-1000	0.9990	13-HODE-d_4
13-OxoODE	88	97.8.0 ± 7.3	0.88 ± 0.12	1.0	1.0–1000	0.9987	13-HODE-d_4
9,10-DiHOME	80	103.0 ± 15.0	1.05 ± 0.15	0.08	0.08-300	0.9991	9,10-DiHOME-d_4
12,13-DiHOME	77	94.2.0 ± 3.4	0.99 ± 0.10	0.04	0.04-300	0.9989	12,13-DiHOME-d_4
9(10)-EpOME	76	91.5 ± 9.5	0.78 ± 0.10	0.5	0.5-1000	0.9999	9,10-DiHOME-d_4
12(13)-EpOME	80	95.0 ± 8.5	0.75 ± 0.11	0.5	0.5-1000	0.9945	9,10-DiHOME-d_4
Resolvin D1	75	94.1 ± 10.4	0.40 ± 0.10	5.0	5.0-1000	0.9998	PGE_2-d_4
Resolvin D2	79	110.0 ± 14.8	0.55 ± 0.12	6.0	6.0-1000	0.9937	PGE_2-d_4
10,17-DiHDoHEA	85	98.0 ± 10.3	0.40 ± 0.08	0.5	0.5-500	0.9960	PGE_2-d_4
19,20-DiHDPA	103	97.2 ± 7.8	5.80 ± 0.75	0.5	0.5-500	0.9948	PGE_2-d_4
17-HDoHE	82	95.2 ± 10.1	1.20 ± 0.20	2.0	2.0–1000	0.9950	12-HETE-d_8
16-HDoHE	78	99.0 ± 3.5	1.25 ± 0.16	2.0	2.0–1000	0.9984	12-HETE-d_8
14-HDoHE	78	93.8 ± 8.8	1.18 ± 0.10	1.0	1.0–1000	0.9989	12-HETE-d_8
13-HDoHE	83	105.0 ± 11.2	1.32 ± 0.20	2.0	2.0–1000	0.9995	12-HETE-d_8
11-HDoHE	77	101.0 ± 8.5	1.15 ± 0.22	2.0	2.0–1000	0.9966	12-HETE-d_8
10-HDoHE	81	88.0 ± 7.8	1.40 ± 0.08	2.0	2.0–1000	0.9984	12-HETE-d_8
8-HDoHE	82	90.2 ± 9.9	1.05 ± 0.15	1.0	1.0–1000	0.9919	12-HETE-d_8
7-HDoHE	79	102.0 ± 8.5	1.20 ± 0.11	1.0	1.0–1000	0.9963	12-HETE-d_8
4-HDoHE	83	108.0 ± 4.5	1.00 ± 0.08	1.0	1.0–1000	0.9994	12-HETE-d_8
6keto-$PGF_{1\alpha}$	85	106.3 ± 8.5	0.95 ± 0.05	0.1	0.1–5000	0.9984	TXB_2-d_4
TXB_2	88	100.2 ± 3.5	1.03 ± 0.03	0.1	0.1–500	0.9990	TXB_2-d_4
$PGF_{2\alpha}$	78	98.1 ± 7.1	0.91 ± 0.03	0.4	0.4–500	0.9988	PGE_2-d_4
$PGF_{1\alpha}$	80	108.2 ± 5.2	2.10 ± 0.03	0.1	0.1–500	0.9917	PGE_2-d_4
PGE_2	77	99.1 ± 4.2	1.02 ± 0.03	0.3	0.3–500	0.9981	PGE_2-d_4
PGE_1	73	103.1 ± 7.1	1.42 ± 0.11	0.2	0.2–500	0.9972	PGE_2-d_4
PGD_2	73	92.1 ± 10.2	0.66 ± 0.07	0.5	0.5–1000	0.9981	PGE_2-d_4
LTB_4	65	98.8 ± 9.1	1.02 ± 0.02	0.7	0.7–1000	0.9992	LTB_4-d_4
20-HETE	76	105.1 ± 3.1	2.20 ± 0.10	0.3	0.3–500	0.9977	12-HETE-d_8
15-HETE	68	97.2 ± 9.2	1.10 ± 0.18	0.6	0.6–1000	0.9953	12-HETE-d_8
12-HETE	66	99.9 ± 8.1	1.00 ± 0.05	0.7	0.7–1000	0.9969	12-HETE-d_8

Analytes	Extraction Yield (%)	Accuracy (% ± SD)	R/R_0	LoQ (pg)	Calibrated range (pg)	Correlation coefficient (r^2)	Internal standard
11-HETE	73	97.9 ± 4.2	1.32 ± 0.13	0.5	0.5–1000	0.9973	12-HETE-d_8
8-HETE	80	103.1 ± 5.5	1.50 ± 0.12	0.5	0.5–1000	0.9972	12-HETE-d_8
5-HETE	70	108.4 ± 7.2	0.82 ± 0.08	0.8	0.8–1000	0.9999	12-HETE-d_8
14,15-EET	75	94.3.1 ± 4.4	0.91 ± 0.11	0.8	0.8–1000	0.9989	12-HETE-d_8
11,12-EET	80	98.9 ± 6.7	0.80 ± 0.08	0.8	0.8–1000	0.9982	12-HETE-d_8
8,9-EET	79	101.0 ± 9.9	0.75 ± 0.14	0.8	0.8–1000	0.9991	12-HETE-d_8
5,6-EET	85	106.2 ± 7.7	0.95 ± 0.08	0.5	0.5–1000	0.9990	12-HETE-d_8

[a] Relative response factor (R/R_0) was calculated as the ratio of an equivalent amount of analyte (R) to its internal standard (R_0) and expressed as the mean ± standard deviation (N=3).

[b] LOQ was defined as 3 × the limit of detection which is expressed as pg injected on column resulting an signal to noise ratio of 3:1.

[c] Method accuracies were calculated as the percent deviation from the expected concentrations and expressed as the mean ± standard deviation (n= 3 experiments).